

DOI: 10.1002/adfm.200701337

Epitaxial Growth of Aligned Semiconductor Nanowire Metamaterials for Photonic Applications**

By Otto L. Muskens, Silke L. Diedenhofen, Maarten H. M. van Weert, Magnus T. Borgström, Erik P. A. M. Bakkers, and Jaime Gómez Rivas*

A novel class of optical metamaterials is presented consisting of high densities of aligned gallium phosphide (GaP) nanowires fabricated using metal-organic vapor phase-epitaxy. Starting from a gold island film as a catalyst for nanowire growth, a sequential combination of vapor-liquid-solid and lateral growth modes is employed to obtain a continuous tunability of the nanowire volume fraction from 7% to over 35%. By choosing different crystallographic orientations of the GaP substrate, metamaterials are designed with different nanowire orientations. The anisotropy of the nanowire building blocks results in strong optical birefringence. Polarization interferometry demonstrates a very large polarization extinction contrast of 4×10^3 combined with a sharp angular resonance which holds promise for optical sensing. Nanowire metamaterials may find applications in photonics, optoelectronics, non-linear and quantum optics, microfluidics, bio-, and gas sensing.

1. Introduction

Artificial materials exhibiting optical, electrical, or mechanical properties that are governed by the arrangement of their microscopic building blocks are of great importance in science and technology. Photonic metamaterials with subwavelength-scale structuring show effective optical properties markedly different from those of their individual constituent materials.^[1] One of these properties is optical form-birefringence, the difference in refractive index for different polarizations of light, resulting from the arrangement of anisotropic scatterers.^[2] Optical form-birefringence has been observed in various systems such as aligned carbon nanotube films,^[3] porous silicon,^[4–6] and liquid-crystal templated porous

CdTe.^[7] In periodic structures like photonic crystals^[8,9] and gratings,^[10] large artificial birefringence occurs at certain frequencies near a resonance dictated by the periodicity. Subwavelength periodic structures in the visible are usually hard to produce and involve complex nanofabrication techniques with tight design tolerances. Novel methods to fabricate photonic materials reproducibly over large areas are of great importance in applications such as liquid-crystal display technology,^[11] integrated photonics,^[12] and optical sensing.^[5,13,14] Artificial metamaterials consisting of porous material at low volume fraction have recently been employed in broadband antireflection coatings.^[14]

Here, we report on the bottom-up fabrication of a novel class of photonic metamaterials based on aligned semiconductor nanowires, exhibiting large artificial birefringence and optical polarization contrast. Semiconductor nanowires are at the focus of a rapidly expanding research field because of their promise as a building block for devices and applications.^[15] For single semiconductor nanowires, large anisotropy of the absorption and emission of light has been demonstrated by polarization-dependent luminescence measurements.^[16] This anisotropy was explained by the different polarizabilities of a thin cylinder for polarizations perpendicular and parallel to its axis. For ensembles of aligned nanowires, polarization anisotropy results in large optical birefringence.^[17] Semiconductor nanowires can be grown heteroepitaxially over large areas on most crystalline substrates including silicon^[18,19] and InP using the versatile bottom-up process of metal-organic vapor phase-epitaxy (MOVPE). Excellent spatial control over local growth allows straightforward integration with waveguides and photonic nanostructures.^[20] The nanowire morphology is complementary to inverted network materials such as porous silicon, which have found important applications in chemistry and biology.^[21] This open morphology of a nanowire

[*] Dr. J. Gómez Rivas, Dr. O. L. Muskens, S. Diedenhofen, M. H. M. van Weert^[+]
FOM Institute for Atomic and Molecular Physics AMOLF
c/o Philips Research Laboratories
High Tech Campus 4, 5656 AE, Eindhoven (The Netherlands)
E-mail: rivas@amolf.nl

Dr. M. T. Borgström,^[++] Dr. E. P. A. M. Bakkers
Philips Research Laboratories
High Tech Campus 4, 5656 AE, Eindhoven (The Netherlands)

[+] Present address: Kavli Institute of Nanoscience, Delft University of Technology, Lorentzweg 1, 2628CJ, Delft, The Netherlands.

[++] Present address: Nanometer Structure Consortium, Lund University, P.O. Box 118, 221 00 Lund, Sweden.

[**] We thank G. Immink, W. van der Einden, and E. Evens for their technical assistance, F. Holthuysen and P. Breijmer for SEM analysis, and M. Verheijen for TEM analysis. This work is part of the research program of the the “Stichting voor Fundamenteel Onderzoek der Materie (FOM)”, which is financially supported by the “Nederlandse Organisatie voor Wetenschappelijk Onderzoek (NWO)”, and is part of an industrial partnership program between Philips and FOM.

Table 1. List of samples with VLS and lateral growth times, nanowire diameter (standard deviation), length, and birefringence Δn .

No.	GaP substrate orientation	VLS growth [min]	Lateral growth [min]	Average diameter (d) [nm]	Length [μm]	Volume fraction [%]	Birefringence Δn [a]
A	(111)B	2	0	19 ± 6	0.3 ± 0.1	–	–
B	(111)B	36	0	27 ± 6	4.6 ± 0.2	8 ± 4	0.047
C	(100)	17	0	22 ± 4	1.2 ± 0.1	7 ± 4	0.003
D	(100)	17	3 min 20 s	31 ± 3	1.3 ± 0.1	15 ± 5	0.011
E	(100)	17	8 min 20 s	43 ± 10	1.4 ± 0.2	25 ± 5	0.099
F	(100)	17	13 min 20 s	72 ± 19	1.5 ± 0.2	35 ± 5	0.209

[a] Systematic error in birefringence values is $\pm 10\%$ of Δn .

ensemble compared to nanometer-sized pores in inverted networks will be superior for applications dealing with large molecules and liquids, for example in microfluidic environments.^[22] Integration of III-V nanowires with silicon^[19] will lead to hybrid nanowire metamaterials that will benefit from existing functionalization methods^[21] while maintaining the electrical and optical properties of the III-V backbone. High-density nanowire metamaterials will also be of importance for next-generation photovoltaic designs.^[23,24]

2. Results and Discussion

2.1. Nanowire Growth

High-density ensembles of gallium phosphide (GaP) nanowires were grown in a MOVPE reactor following the procedure outlined in Section 4. The substrate is a single-crystalline GaP wafer covered with a 3-Å thin gold film. The gold film provides a homogeneous coverage of the whole surface with small, uniformly distributed islands.^[25] Catalytic growth using the vapor–liquid–solid (VLS) process^[26–28] results in nanowires with a diameter determined by the size of the catalyst particles. The length of nanowires is set via the VLS growth time. Subsequently, the photonic strength of the material is tuned via the diameter of the wires by switching from the vapor–liquid–solid to the lateral growth mode. In this step, the nanowire layer is gradually filled up with semiconductor material at a higher temperature (630 °C) of the MOVPE chamber where the kinetic hindrance is overcome. The lateral growth process is limited by diffusion of precursor gases into the dense nanowire layer, which in practice limits this approach to nanowires shorter than 2 μm . Table 1 gives an overview of the nanowire materials of this study, grown on various substrate orientations using a combination of VLS and lateral growth.

2.2. Structural Characterization

The morphology of the nanowire materials was investigated using both top-view and cross-sectional scanning electron microscopy (SEM). Figure 1a shows a top-view SEM image of sample A, after a very short period of VLS growth. The image reveals a density of nanowire growth centers of around 390 sites per μm^2 . The histogram of diameters (Fig. 1c) shows a lognormal distribution around an average of 18.7 nm. Since sites smaller than ~ 10 nm cannot be discerned in the SEM image, the measured distribution is slightly biased toward larger diameters. The volume fraction of growth centers per unit area is estimated as $(12 \pm 2)\%$ on the basis of SEM contrast analysis.

Gallium phosphide nanowires of several micrometers in length were grown by increasing the VLS growth time to

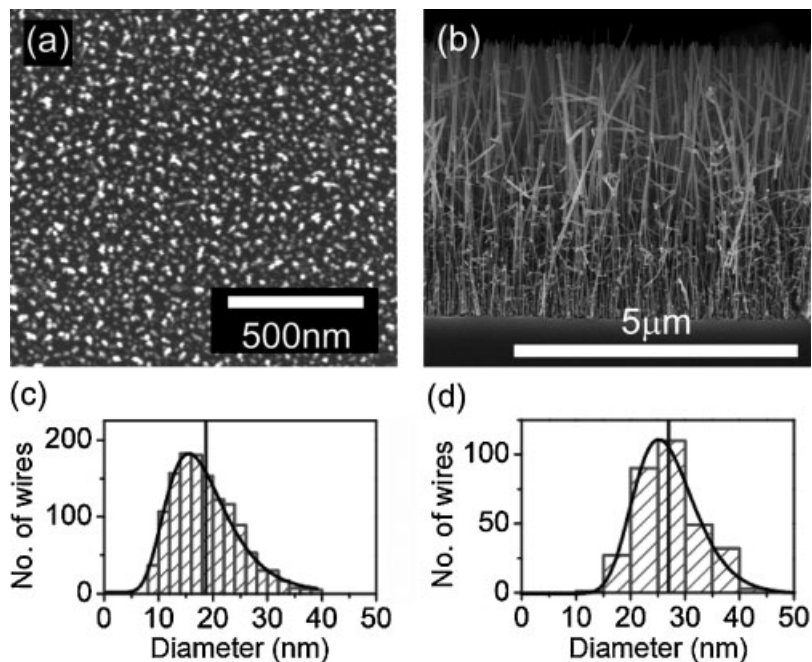


Figure 1. a) Scanning electron micrograph (top view) of nanowire nucleation sites on sample A. b) Cross-sectional SEM micrograph of a cleaved section of sample B. c, d) Size histograms of the nucleation sites and nanowires with lognormal fits (lines).

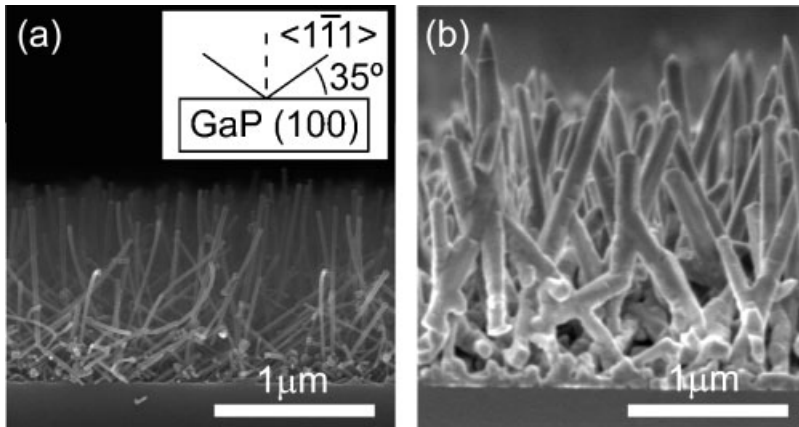


Figure 2. a) Cross-sectional SEM image of a cleaved (110)-section of nanowire metamaterial C, with (inset) schematic overview of crystallographic growth direction of the nanowires on the (100) GaP substrate. b) Same for material F.

sectional SEM images of GaP nanowires grown from a GaP (100) substrate, for a section cleaved along the (110)-plane. This cleaving orientation provides a projection perpendicular to the growth plane of the $\langle 111 \rangle$ B nanowires, i.e., the wires are oriented in the plane of the SEM image. We observe a high-density distribution of nanowires with a large fraction of the wires under an angle of around 35° with respect to the surface of the substrate. Some wires are observed that are oriented in the $\langle 100 \rangle$ direction, and some in higher order $\langle 11x \rangle$ B directions ($x > 1$). The preferential growth will be exploited in Sections 2.4 and 2.5 to control the direction of the optical axis, and thus the birefringence, in the nanowire material. The average wire diameter for these materials was determined from SEM images and is shown in Table 1. From these

36 min. Figure 1b shows a cross-sectional SEM image of the nanowire layer grown on a (111)B GaP substrate. The nanowires are aligned perpendicular to the substrate due to the preferential growth in the $\langle 111 \rangle$ B direction. The thin wires show some bending toward the top, probably caused by an enhanced flexibility of the semiconductor material at these very small diameters. The distribution of nanowire diameters obtained from the SEM image is presented in Figure 1d, showing a distribution centered around a diameter of 27 nm, with a polydispersity given by the standard deviation of $\pm 20\%$. The nanowire size distribution is comparable to that of the nucleation sites in Figure 1a, indicating that the nanowire diameter is determined by the metal catalyst particle. In Figure 1b as well as in top-view SEM images (not shown), the nanowire volume fraction appears lower than the initial density of growth centers which we assign to competitive growth and spontaneous growth interruption of wires. From the number density and diameters of full-grown wires we estimate a volume fraction of $(8 \pm 4)\%$ as shown in Table 1. This value is corroborated by gravimetric analysis of the sample before and after growth.

The preferential growth of GaP nanowires in the $\langle 111 \rangle$ B direction was used to obtain nanowire ensembles with nonvertical orientations by changing the crystallographic orientation of the substrate. Figure 2a shows cross-

diameters we have estimated the increase in volume fraction of the layers upon lateral growth, as indicated in Table 1.

The crystalline properties of nanowires fabricated using VLS and lateral growth were analyzed using transmission electron microscopy (TEM) and energy dispersive X-ray

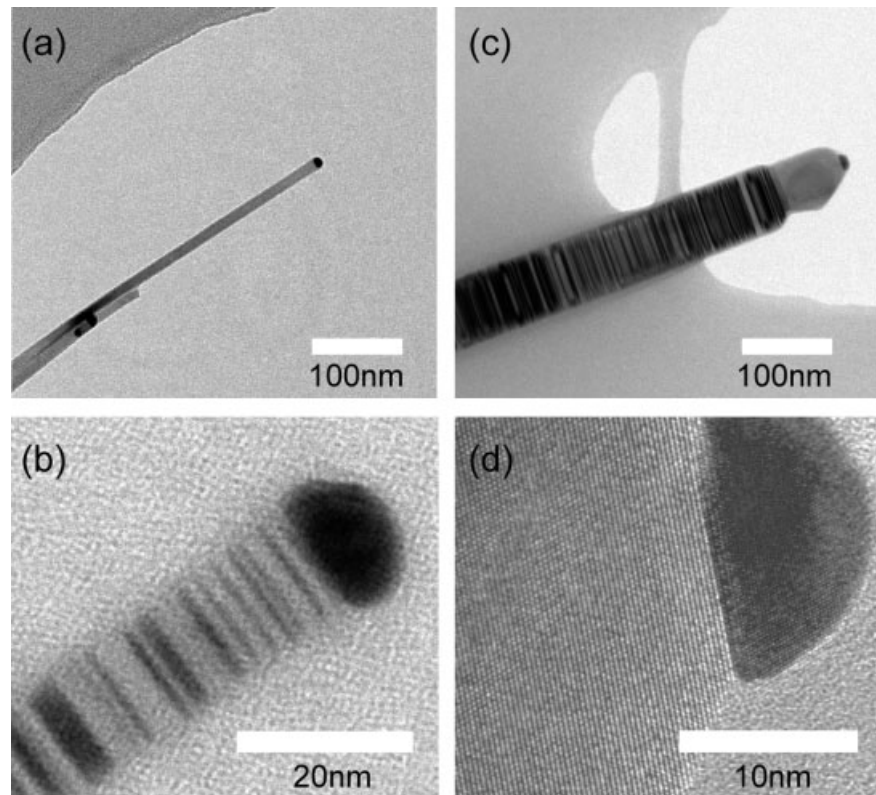


Figure 3. Brightfield transmission electron microscopy (TEM) image of GaP nanowires originating from a, b) layer C and c, d) layer F. b, d) HRTEM images of nanowire tips showing crystalline structure. The small dark region at the tip of each nanowire indicates the gold catalyst particle which remains located on top of the wire during growth.

(EDX) analysis. Figure 3 shows TEM micrographs of wires taken from the (100) GaP metamaterials C (a,b) and F (c,d) of Table 1. The wires from material C have diameters ranging from approximately 10 to 20 nm, no tapering was observed. The wires from material F, with additional lateral growth, are considerably thicker: diameters exceeding 80 nm are observed. The diameter of the original gold particle (see Fig. 3b and d) gives a good indication of thickness prior to sidewall growth. The contrast lines, orthogonal to the length direction of the wires, observed for both the thin and the thick wire, correspond to twin domains with alternating orientations along the $\langle 111 \rangle$ axis of the wire. Remarkably, the upper segment of the wire in Figure 3c is free of twin boundaries. The presence of a single-crystalline end-segment was observed only for nanowires from sample F, indicating that this 100-nm long segment results from competing VLS growth during the lateral growth step. The nanowires have the zinc-blende structure, as determined from fast-Fourier-transforms of HRTEM images such as that in Figure 3d. EDX studies of an area containing a group of nanowires (without any gold particles included) revealed Ga and P with equal stoichiometry. A more detailed TEM analysis of GaP nanowire growth using the same MOVPE-system was presented in Ref. [28].

2.3. Optical Characterization

An important application of porous form-birefringent materials is as an optical sensor using polarization interferometry.^[4–6] The resolution of such a device depends strongly on the strength of the birefringence and on the contrast between the orthogonal polarization states. The goal of our research is to fabricate a metamaterial that combines a very large optical anisotropy in the optical frequency domain with a high degree of polarization contrast. In order to achieve this combination we have chosen to use gallium phosphide (GaP) nanowires. Gallium phosphide combines the largest refractive index in the visible of around 3.4 with very low absorption below its indirect electronic bandgap located at 2.26 eV (548 nm).^[29] The polarizability of nanowires strongly depends on their orientation with respect to the optical field. As a consequence, nanowires show a large anisotropy in their optical response.^[16,17,30] Here, we investigate the optical properties of nanowire layers as a function of their density and alignment.

An ideal optical metamaterial consists of scattering building blocks that are much smaller than the optical wavelength in the medium. Under this condition the arrangement of scatterers results in a material with a refractive index determined by effective medium theory. To test this assumption for the nanowire metamaterials under study, we have performed

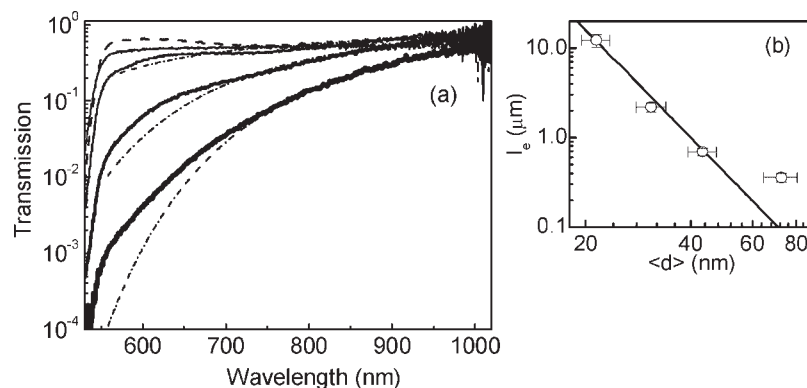


Figure 4. a) Transmission spectrum of a white light beam through a GaP substrate (dashed line) and (100) GaP nanowire metamaterials C (thin line) – F (thick line) with increasing nanowire diameters. Dash-dotted lines are fits using Rayleigh scattering model. b) Extinction mean free path l_e at 690 nm wavelength for materials C–F, (line) fit proportional to $\langle d \rangle^{-4}$.

white-light transmission spectroscopy using the procedure described in Section 4. Figure 4a shows the transmission spectra for samples C–F together with a bare (100) GaP substrate (dashed line). For all samples, a sharp absorption edge is present due to the electronic bandgap of GaP at 548 nm. The reference sample shows an overall flat transmission below 100 % due to Fresnel reflection losses, with a slight interference contribution from a thin-film SiO₂ protective coating at the backside of the substrate. For the samples C–F with increasing lateral growth times, a strongly wavelength dependent transmission is observed, which can be assigned to Rayleigh scattering of the thin nanowires (dash-dotted lines), as shown below. The scattering losses increase considerably for thicker nanowires and toward shorter wavelengths. Above 900 nm, the optical transmission is only slightly reduced with respect to the bare substrate.

We have interpreted the strong wavelength dependence of the transmission through the nanowire material using a simple Beer's law for the coherent beam assuming Rayleigh scatterers, given by

$$T = T_0 \exp(-L/l_e), \quad (1)$$

where T_0 denotes the Fresnel transmission coefficient through the layer, $l_e(\lambda) = A \lambda^4$ is the wavelength dependent scattering length containing the typical fourth power dependence on wavelength (Rayleigh scattering), and L denotes the sample thickness. Fits to the data are indicated by the dash-dotted lines in Figure 4a, which show good agreement for wavelengths above 700 nm. For shorter wavelengths deviations arise because of the breakdown of the Rayleigh scattering approximation for finite size scatterers. Figure 4b represents the extinction mean free path at the wavelength of the experiments below, $\lambda = 690$ nm. For a small cylindrical particle in the long-wavelength limit, the scattering mean free path is expected to vary as the

inverse fourth power of the diameter.^[31] This dependence is shown as a line in the inset Figure 4b and gives good agreement for the thin nanowire materials with average wire diameters below $\langle d \rangle = 50$ nm. For the thicker nanowires, finite size effects result in a more complex dependence of the scattering cross-section on particle diameter and wavelength.^[31]

2.4. Angle-Dependent Polarization Interferometry of Nanowires on a (111)B GaP Substrate

For a material consisting of vertically aligned semiconductor nanowires, the polarization directions perpendicular to the wire axis have a lower refractive index than the direction parallel to the nanowires.^[2] An optical beam traveling through this material will therefore have a different velocity depending on its polarization. We used the method of polarization interferometry as explained in Section 4 to investigate the birefringence in the nanowire materials. Due to the preferential orientation of the wires on the (111)B substrate, the optical birefringence is expected to vary strongly between normal and in-plane incidence of light. The ratio of intensities in the cross-polarized I_{\perp} and parallel polarized I_{\parallel} transmission channels is a measure for the degree of rotation of the polarization vector. This method, closely related to the more general technique of ellipsometry, has been widely used for the determination of optical birefringence as well as in optical sensors.^[4–6] Figure 5a shows this intensity contrast I_{\perp}/I_{\parallel} over more than 4 orders of magnitude for the nanowire material B. For comparison we have also plotted the result for a bare GaP (111)B substrate. Bulk GaP itself has only very small intrinsic birefringence ($<10^{-5}$),^[32] which gives a negligible contribution to the retardation. The small change in the ratio for the

bare substrate can be completely explained by the difference in Fresnel transmission coefficients for the in-plane (p-) and out-of-plane (s-) polarizations, leading to a distortion of the initial polarization state. The nanowire material shows a much stronger dependence on angle, with a maximum occurring at 72° . This maximum corresponds to half-wavelength retardation, where the polarization vector has been converted entirely to the cross-polarized state. The amplitude of this maximum in I_{\perp}/I_{\parallel} is determined by the suppression of the original parallel state I_{\parallel} . By correcting the input state for polarization-dependent reflection losses, we have been able to further improve the maximum contrast by two orders of magnitude, as shown by the thin line in Figure 5a. This increase of the amplitude is associated with a narrowing of the full-width-at-half-maximum of the maximum from 9° to 1.1° .

The intensity ratio I_{\perp}/I_{\parallel} for the reflected light is shown in Figure 5b. The effect of nanowire birefringence on the polarization state is here two times larger than in transmission since the optical beam passes through the nanowire layer twice. As a consequence, the location of the maximum in the intensity ratio occurs at an angle of incidence of 54° . Again a sharp maximum in the contrast is obtained after correction of the input state, with an extinction of the orthogonal polarization exceeding 4×10^3 . This value exceeds the measured ratio in transmission, which we attribute to a reduced scattering background at smaller angles of incidence. Both the stronger angle-dependence of the intensity ratio and the higher extinction result in a reduced full-width-at-half-maximum of 0.45° . At angles above 60° , a complex oscillation pattern arises that can be assigned to thin-film interference fringes in the nanowire layer. These fringes distort the effects of retardation at large angles.

Accurate estimates of the material refractive indices for the (111)B GaP nanowires in Figure 5 were obtained by fitting the angle-dependent transmission using a transfer matrix model accounting for Fresnel reflections at the various interfaces and for the uniaxial birefringence of the nanowire layer. The results of these fits are represented by the thin black lines in Figure 5 and show good quantitative agreement with the experimental results. The resulting birefringence coefficient Δn was determined as 0.047 ± 0.005 , where the error bar results from the uncertainty in the optical thickness of the birefringent layer.

To investigate the use of angle-dependent nanowire birefringence for optical sensing we calculated the change of the contrast function for a small change of the birefringence parameter. The result is given in Figure 6a and b. Again the reflectivity contrast of Figure 5b is plotted around the maximum, but now with a fit including the correction for the input polarization (dashed line, black). Figure 6b compares this fit to a calculation using the same parameter except for a small change in

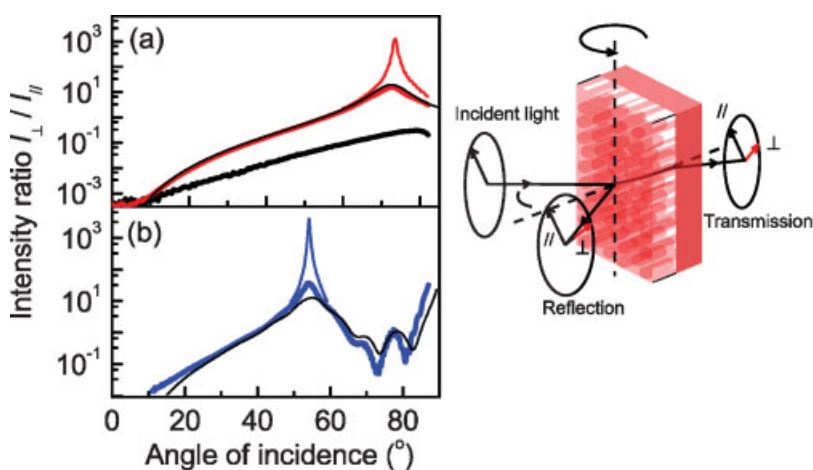


Figure 5. a) Transmission intensity ratio I_{\perp}/I_{\parallel} as a function of the angle of incidence for sample B (red line) and for a bare GaP substrate (thick black line). (The thin black line denotes a fit using a transfer-matrix model of a birefringent layer. b) Ratio I_{\perp}/I_{\parallel} for the specular reflected light for sample B (blue line) and model fit (thin black line). Thin colored lines in (a) and (b) are measurements after optimization of the input polarization minimizing I_{\parallel} (see text). The sketch shows the experimental configuration.

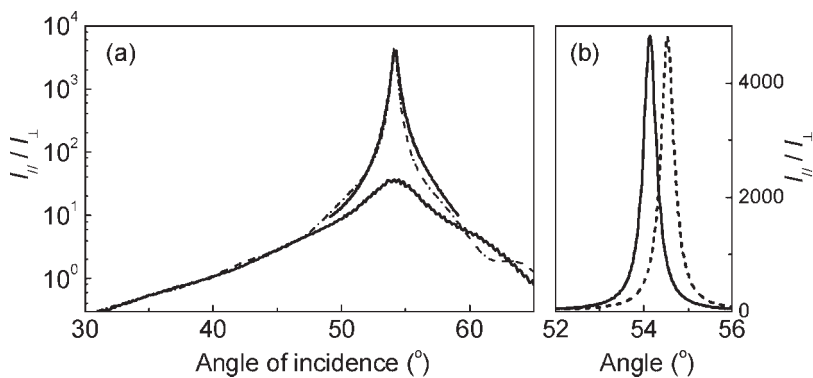


Figure 6. a) Experimental (thick lines) and calculated (dash-dotted line) reflection contrast of sample B. b) Calculated values around maximum at 54.1° (linear scale) for a birefringence $\Delta n = 0.047$ (line) and for $\Delta n = 0.046$ (dashed line).

birefringence Δn of 10^{-3} . We find a displacement of the contrast maximum over an angle of 0.5° , i.e., one linewidth of the interferometric peak structure. We estimate that much smaller changes, i.e., below 10^{-4} , will be measurable using sensitive differential techniques on the slope of the peak. This corresponds well to sensitivities reported for porous silicon, in principle allowing for sensing of molecules in the ppm range.^[6]

2.5. In-Plane Birefringence of Nanowires on a (100) GaP Substrate

To demonstrate the versatility of the bottom-up fabrication of nanowire photonic materials, we controlled the direction of the birefringence using the special crystallographic growth directions of semiconductor nanowires. Conclusive evidence of this preferential nanowire orientation is given by the optical birefringence experiment presented in Figure 7 and explained

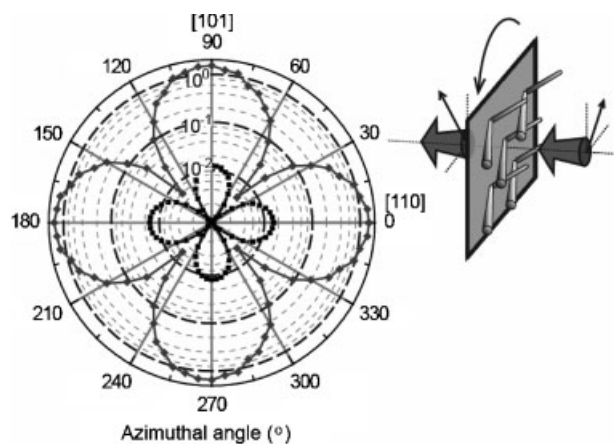


Figure 7. Transmitted intensity ratio I_{\perp}/I_{\parallel} at a wavelength of 690 nm, as a function of the azimuthal orientation of the birefringent nanowire layer, for GaP nanowires C (black squares) and F (grey diamonds) grown on (100) GaP (see Fig. 2a and b). Sketch shows experimental configuration.

in Section 4. Here the transmission of a normally incident wave on the sample is measured while rotating the nanowire sample azimuthally, i.e., around the normal of the sample surface. We observe a typical fourfold pattern that is indicative of in-plane birefringence as can be understood using simple arguments. At -45° and 45° azimuthal angle the nanowires are aligned respectively parallel and perpendicular to the incident polarization vector, therefore no retardation takes place. This results in a zero of the ratio I_{\perp}/I_{\parallel} . At 0° and 90° azimuthal angle, the fast optical axis of the nanowires is at 45° with the input polarization, giving rise to retardation and hence to a maximum in the ratio I_{\perp}/I_{\parallel} . The amount of retardation is relatively small for thin wires (sample C) but increases strongly with increasing nanowire filling fraction (sample F).

For sample F a maximum ratio I_{\perp}/I_{\parallel} larger than unity is obtained, indicating that we have fabricated an in-plane quarter-wavelength retarder using semiconductor nanowires (cf. Sec. 4).

From the retardation, denoted here as δ , we can derive the in-plane birefringence using the definition^[2,5] $\delta = \Delta n L$, where L denotes the thickness of the nanowire layer. The retardance can be obtained from the contrast ratio via the relation $(I_{\perp}/I_{\parallel})_{\max} = \tan \pi \delta / \lambda$, where λ is the wavelength in vacuum, resulting in the values of the birefringence parameter Δn presented in Table 1. The error in the obtained birefringence values is mainly determined by an uncertainty in the layer thickness resulting from the various growth directions of nanowires on (100) GaP, as observed in Figure 2a and b.

From the maximum ratio of $I_{\perp}/I_{\parallel} = 1.5$ for the (100) GaP nanowire material F in Figure 7, we calculate a retardation over $\lambda/4$, hence the nanowires act as a quarter waveplate retarder at an optical wavelength of 690 nm. Between the materials C–F before and after additional lateral growth, we find a variation over 2 orders of magnitude in the birefringence value Δn . The lateral growth step results in a significant increase of the nanowire volume fraction by more than a factor of five. From effective medium theories such as Maxwell–Garnett^[17] or Bruggeman,^[6] we may expect a concomitant increase of the optical anisotropy in the low-volume fraction regime. For the thin-wire samples C and D, there is still an additional reduction of birefringence by almost an order of magnitude that is not accounted for by effective medium models. We expect that this reduction is due to orientational disorder in the layer which is more pronounced for thin wires due to their abovementioned flexibility.^[17] Note that in these calculations we did not include effects from scattering, since to first order these are not expected to affect the polarization properties of the coherent beam. In the analysis, the specific Y-shaped morphology of the nanowires on (100) GaP is not taken into account since we only consider light incident perpendicular to the surface. For the optical response at

oblique angles of incidence, a more detailed analysis, including the full, three-dimensional nanowire orientations, will be required, which goes beyond the current investigation.

3. Conclusions

We have demonstrated that bottom-up fabrication of epitaxially-grown, semiconductor nanowires using MOVPE yields highly anisotropic photonic metamaterials. We have demonstrated control over both the morphology and the alignment of the nanowire metamaterials using a combination of VLS- and lateral growth and by growing on substrates with different crystallographic orientations. Using white light transmission measurements, we have observed a strongly wavelength-dependent optical extinction, following Rayleigh scattering at long wavelengths and for small nanowire diameters. For nanowire diameters above 50 nm a transition is found to the non-Rayleigh scattering regime. Although the short scattering mean free paths may pose limitations for application as optical elements, it may also be advantageous for trapping light inside structures such as solar cells and photodetectors. The exploration presented here may therefore be relevant for future designs and concepts in those areas.

In the polarization interferometry experiment, vertically aligned nanowire layers show very sharp features with a high dynamic range both in angular-dependent transmission and in reflection. In the latter configuration the effect of birefringence is twice as large due to the double passage through the layer. However, this configuration also suffers more strongly from spurious reflections and thin-film Fabry–Pérot fringes. The very high dynamic range of 10^6 combined with high angular resolution make polarization interferometry an ideal tool for optical sensing. The sharp features obtained for long and thin nanowire samples are highly promising and at least comparable to the porous silicon materials used in earlier work.^[5,6,33] The fact that GaP phosphide has a relatively high-energy bandgap therefore allows a significant extension into the visible spectrum. The MOVPE method allows us to reproduce these nanowire layers in a controlled way, yielding constant optical birefringence values within the experimental error of 10% between runs.

Although we focused our investigation on gallium phosphide nanowires, nanowire metamaterials can be grown using any group III-V, II-VI, or IV semiconductor on any crystalline surface, offering the possibility of visible, near- and mid-infrared birefringence. Advantages of the bottom-up fabrication of the photonic nanowire birefringent materials are the high degree of control over local growth, the possibility of large area growth without the need of complex nanofabrication techniques, and the compatibility of the growth with silicon technology.

4. Experimental

MOVPE Fabrication of Nanowire Layers: A gallium phosphide (GaP) substrate was used with both sides mechanically and chemically polished to optical quality. A 500-nm SiO₂ was deposited on the back

surface using plasma deposition to prevent rough etching of this side. The substrate was etched in HNO₃:HCl:H₂O (2:3:3) at 80 °C for 2 min. Immediately after this step, a gold film with a thickness of 3 Å was deposited on the front surface, which was either a P-terminated (111)B or a (100) interface. Subsequently the samples were transferred to a low-pressure (50 mbar) MOVPE system (Aixtron 200). Epitaxially oriented nanowires were grown in the VLS growth mode at an elevated temperature of 420 °C using trimethylgallium (TMG) and phosphine (PH₃) with molar fractions of $\chi_{\text{TMG}} = 9.1 \times 10^{-5}$ and $\chi_{\text{PH}_3} = 15.0 \times 10^{-3}$ respectively, as precursors in a total flow of 6.01 min⁻¹ using hydrogen (H₂) as carrier gas. Radial growth on the nanowire sidewalls was carried by switching off TMG during a temperature ramp to 630 °C after which the TMG flow was reintroduced into the reactor. After growth, the samples were cooled down in a PH₃ containing atmosphere.

Characterization: SEM images were made using a Nova NanoSEM 600 microscope by FEI Company. TEM, HRTEM, and EDS studies were performed using a Tecnai F30ST microscope at 300 kV. Individual nanowires were obtained from the layer by wiping of the sample over a copper grid. Statistical analysis of SEM images was done using ImagePro software. The diameter distribution of nucleation sites was obtained from contrast-analysis of the SEM image, yielding the area per nucleation site. Effective diameters were obtained from these areas using a cylindrical approximation, while the error was estimated from the uncertainty in the contrast threshold. The distribution of nanowire diameters was obtained by measuring, by hand, the diameters of 100 individual nanowires in the SEM images using the ImagePro software.

Optical Characterization: Optical transmission spectra were measured using a Yokogawa AQ4303 fiber-coupled white light source. The fiber output was collimated using an achromatic objective and impinged perpendicular to the nanowire layer. Broadband polarization filters were used to select the incident and detected polarization states. The spectrum of transmitted light was measured using an Ocean Optics USB2000 spectrometer. A dynamic range of 10⁴ was obtained by combining two spectra with acquisition times of 0.1 and 2 s. All transmission spectra were normalized to the spectrum of the white-light incident beam.

Angle-Dependent Polarization Interferometry: The experimental scheme followed the general procedure presented in Refs. [4–6] and consisted of an angle-dependent reflection and transmission setup with a resolution of 0.1° and polarization sensitivity of 1:10³. A 632.8 nm He:Ne laser and a 690 nm diode laser were used for the experiments. The polarization of the input beam was set to 45° with respect to the plane of incidence. The rotation of the polarization vector after propagation through the nanowire layer was measured via the parallel- (I_{\parallel}) and cross-polarized (I_{\perp}) intensities (relative to the input polarization). The angle of incidence of the light was varied between 0 and 90°. The rotation of the polarization vector due to retardation inside the nanowire layer is measured via the polarization ratio I_{\perp}/I_{\parallel} . A pole in this ratio indicates a complete conversion of the original polarization state to a linear polarized orthogonal state, i.e., a retardation of $\lambda/2$. Retardation of $\lambda/4$ results in circular polarized output light, hence an equal contribution of the original and orthogonal state, which is measured as an I_{\perp}/I_{\parallel} ratio of 1. For the (100) GaP materials, the polarization ratio was measured as a function of the azimuthal orientation of the nanowire layer.

Received: November 15, 2007

Revised: January 24, 2008

Published online: March 31, 2008

[1] N. Engheta, R. W. Ziolkowski, *Electromagnetic Metamaterials: Physics and Engineering Explorations*, 1st ed., Wiley, New York 2006.

- [2] M. Born, E. Wolf, *Principles of Optics*, 6th ed., Cambridge University Press, Cambridge **1997**, p. 665.
- [3] W. A. De Heer, W. S. Bacsá, A. Chatelain, T. Gerfin, R. Humphrey-Baker, L. Forro, D. Ugarte, *Science* **1995**, *268*, 845.
- [4] N. Künzner, D. Kovalev, J. Diener, E. Gross, V. Y. Timoshenko, G. Polisski, F. Koch, M. Fujii, *Opt. Lett.* **2001**, *26*, 1265.
- [5] E. Gross, D. Kovalev, N. Künzner, V. Y. Timoshenko, J. Diener, F. J. Koch, *J. Appl. Phys.* **2001**, *90*, 3529.
- [6] B. O. R. Liu, Y. Y. Li, M. J. Sailor, Y. Fainman, *IEEE Photon. Technol. Lett.* **2003**, *15*, 834.
- [7] M. F. Weber, C. A. Stover, L. R. Gilbert, T. J. Nevitt, A. J. Oudekirk, *Science* **2000**, *287*, 2451.
- [8] F. Genereux, S. W. Leonard, H. M. Van Driel, A. Birner, U. Gösele, *Phys. Rev. B* **2001**, *63*, 161101.
- [9] H. Kosaka, T. Kawashima, A. Tomita, M. Notomi, T. Tamamura, T. Sato, S. Kawakami, *Phys. Rev. B* **1998**, *58*, R10096.
- [10] F. Xu, R.-C. Tyan, P.-C. Sun, Y. Fainman, C.-C. Cheng, A. Scherer, *Opt. Lett.* **1995**, *20*, 2457.
- [11] E. Peeters, J. Lub, J. A. M. Steenbakkens, D. J. Broer, *Adv. Mater.* **2006**, *18*, 2412.
- [12] M. V. Kotlyar, L. Bolla, M. Midrio, L. O'Faolain, T. F. Krauss, *Opt. Express* **2005**, *13*, 5040.
- [13] S. E. Létant, M. J. Sailor, *Adv. Mater.* **2001**, *13*, 335.
- [14] J.-Q. Xi, M. F. Schubert, J. K. Kim, E. F. Schubert, M. Chen, S.-Y. Lin, W. Liu, J. A. Smart, *Nature Photon.* **2007**, *1*, 176.
- [15] a) Y. Li, F. Qian, J. Xiang, C. M. Lieber, *Mater. Today* **2006**, *9*, 18.
b) P. J. Pauzauskie, P. Yang, *Mater. Today* **2006**, *9*, 36.
- [16] J. Wang, M. K. Gudiksen, X. Duan, Y. Cui, C. M. Lieber, *Science* **2001**, *293*, 1455.
- [17] O. L. Muskens, M. T. Borgström, E. P. A. M. Bakkers, J. Gómez Rivas, *Appl. Phys. Lett.* **2006**, *89*, 233117.
- [18] T. Mårtensson, C. P. T. Svensson, B. A. Wacaser, M. W. Larsson, W. Seifert, K. Deppert, A. Gustafsson, L. R. Wallenberg, L. Samuelson, *Nano Lett.* **2004**, *4*, 1987.
- [19] E. P. A. M. Bakkers, J. A. Van Dam, S. De Franceschi, L. P. Kouwenhoven, M. Kaiser, M. Verheijen, H. Wondergem, P. Van der Sluis, *Nat. Mater.* **2004**, *3*, 769.
- [20] A. I. Hochbaum, R. He, R. Fan, P. Yang, *Nano Lett.* **2005**, *5*, 457.
- [21] M. P. Stewart, J. M. Buriak, *Adv. Mater.* **2000**, *12*, 859.
- [22] H. D. Tong, H. V. Jansen, V. J. Gadgil, C. G. Bostan, E. Berenschot, C. J. M. van Rijn, M. Elwenspoek, *Nano Lett.* **2004**, *4*, 283.
- [23] M. Law, L. E. Greene, J. C. Johnson, R. Saykally, P. Yang, *Nat. Mater.* **2005**, *4*, 455.
- [24] B. Tian, X. Zheng, T. J. Kempa, Y. Fang, N. Yu, G. Yu, J. Huang, C. M. Lieber, *Nature* **2007**, *449*, 885.
- [25] I. Doron-Mor, Z. Barkay, N. Filip-Granit, A. Vaskevich, I. Rubinstein, *Chem. Mater.* **2004**, *16*, 3476.
- [26] R. S. Wagner, W. C. Ellis, *Appl. Phys. Lett.* **1964**, *4*, 89.
- [27] E. I. Givargizov, *J. Cryst. Growth* **1975**, *31*, 20.
- [28] M. A. Verheijen, G. Immink, T. De Smet, M. T. Borgström, E. P. A. M. Bakkers, *J. Am. Chem. Soc.* **2006**, *128*, 1353.
- [29] E. D. Palik, *Handbook of Optical Constants of Solids*, 1st ed., Academic, Orlando **1985**, p. 445.
- [30] O. L. Muskens, J. Treffers, M. T. Borgström, E. P. A. M. Bakkers, J. Gómez Rivas, *Opt. Lett.* **2007**, *32*, 2097.
- [31] C. F. Bohren, D. R. Huffman, *Absorption and Scattering of Light by Small Particles*, 1st ed., Wiley-VCH, Weinheim **1998**, p. 141.
- [32] J. H. Burnett, Z. H. Levine, E. L. Shirley, *Phys. Rev. B* **2001**, *64*, 241102.
- [33] V. S.-Y. Lin, K. Motesharei, K. S. Dancil, M. J. Sailor, M. R. Ghadiri, *Science* **1997**, *278*, 840.